Journal of Alloys and Compounds 500 (2010) 117–124

Contents lists available at ScienceDirect

Journal of Alloys and Compounds

journal homepage: www.elsevier.com/locate/jallcom

Enhancement of thermal stability of multiwalled carbon nanotubes via different silanization routes

B. Scheibe*, E. Borowiak-Palen, R.J. Kalenczuk

Centre of Knowledge Based Nanomaterials and Technologies, Institute of Chemical and Enviroment Engineering, West Pomeranian University of Technology, Szczecin, Poland

ARTICLE INFO

Article history:
Received 12 November 2009
Received in revised form 26 March 2010
Accepted 31 March 2010
Available online 8 April 2010

Keywords:
Nanostructured materials
Surfaces and interfaces
Thermal analysis

ABSTRACT

This work presents an effect of two different silanization procedures on thermal and structural properties of oxidized and oxidized followed by sodium borohydrate ($NaBH_4$) reduction of multiwalled carbon nanotubes (MWCNTs). Purified sample was oxidized in a mixture of nitric and sulfuric acids in a reflux. An oxidized material was divided into two batches. The first batch underwent a silanization procedure directly, while the second batch was reduced by $NaBH_4$ treatment prior to the silanization. The silanization experiments were performed: (A) with γ-aminopropyltriethoxysilane (APTES) at room temperature in acetone (pH ~7) and (B) with condensated γ-aminopropyltriethoxysilane at 40 °C in water (pH 4). The extent of the functionalization of the samples after each procedure was examined by Raman spectroscopy. The vibrational properties of the materials were studied via Fourier transform infrared spectroscopy. Boehms titration technique was applied to quantify the amount of the functional groups on MWCNTs. The morphology of the pristine and functionalized carbon nanotubes was exposed to high-resolution transmission electron microscopy analysis. The energy dispersive X-ray (EDX) analysis was used to characterize the elemental composition of each sample. The effect of the silanization process on the thermal properties of MWCNTs was investigated by thermogravimetry analysis. Interestingly, the significant increase of the thermal stability of silanized MWCNTs samples in respect to the pristine MWCNTs was observed.

1. Introduction

Since their discovery, a lot of effort has been launched into functionalization of the carbon nanotubes (CNTs) in order to take advantage of their unique properties. Recently, CNTs were intentionally modified in order to perform an exact role in certain applications in such fields as metal and polymer composites [1–7], electrodes [8–11] or sensors [12,13]. Modern modifications of multiwalled carbon nanotubes (MWCNTs) involve single to several steps of the external walls modification, called exohedral functionalization, which depends on further applications of the prepared material [2,14–18]. The oxidation process is the simplest and most common single-step of the outer wall functionalization, leading to the introduction of the functional groups on their outer walls, which can be used as a linkers for further more sophisticated modifications [19–23]. The silanization process is the effective procedure for further modification of the physical and chemical properties of multiwalled carbon nanotubes for present polymer nanocomposites development [7,24]. This modification method involves high concentration of the hydroxyl moieties which act as the anchoring points in the wall's structure and can be obtained via $NaBH_4$ or $LiAlH_4$ reduction of carbonyl and lactone functional groups previously introduced by the oxidation process [20,25]. So far the silanization process was investigated and utilized in many different applications, such as solubility improvement of CNTs, polymer nanocomposites and biosensors [26–32]. However, there was no comprehensive reports describing in great details the influence of the silanization routes on oxidized and reduced MWCNTs sample. Modification of the MWCNTs exohedral surface via silanization process is a complex process and does not involve a single mechanism. The reactivity of the aminosilane molecule to the inorganic surface depends on the reaction time, pH and nature of the solvent, temperature and silane concentration [33]. The aminosilane molecule, composed of hydrolytically stable bond $H_2N–CH_2)_3–Si$ and $Si–(OC_2H_5)_3$, can easily undergo the hydrolysis process due to pH, temperature or aqueous solvent to form a trisilanol. It is known that those groups readily react with the hydroxyl groups on the nanotube surface [33]. In this study, two silanization procedures were used to deposit γ-aminopropyltriethoxysilane on the oxidized and oxidized followed by the reduction of MWCNTs surface. In the first approach (Experiment A) the silanization occurs in one step. The APTES was placed in anhydrous MWCNTs solu-

* Corresponding author at: Department of Nanotechnology, Institute of Chemical and Enviroment Engineering, West Pomeranian University of Technology, Pulaskiego 10, 70-322 Szczecin, Poland.
E-mail address: bscheibe@zut.edu.pl (B. Scheibe).

0925-8388/$ – see front matter © 2010 Elsevier B.V. All rights reserved.
doi:10.1016/j.jallcom.2010.03.229

tion of acetone at room temperature and which was magnetically stirred for 0.5 h. In this way the aminosilane molecules were grafted into MWCNTs defect sites containing hydroxyl groups. In the second approach (Experiment B) the silanization occurs in two steps. Firstly, the APTES was placed into an acid MWCNTs aqueous solution at 40 °C in an ultra-sonication bath for 3 h. The experimental conditions of the second approach promote the hydrolysis process of the ethoxy groups. In the hydrolysis reaction, ethoxy groups (OC_2H_5) are replaced by hydroxyl groups (OH) to form reactive trisilanol groups. The silanols self-condense producing siloxane bonds (Si–O–Si) and form water insoluble aminopropyl-functional resinous oligomers and polymers. The by-products of the condensation process are alcohol and water. Secondly, the polymer which associated with the multiwalled carbon nanotubes surface, formed a covalent bond in defect sites with OH groups. A schematic simplified representation of the experimental steps is shown in Fig. 1.

The detailed spectroscopic, microscopic along with thermogravimetric analysis of the prepared samples were performed. Interestingly, it was detected that the thermal stability of the silanized MWCNTs samples in respect to the pristine (purified) MWCNTs significantly increased. To the best of our knowledge this is the first detailed report on the influence of the silanization process on the thermal stability of these molecular hybrids.

2. Experimental

2.1. Materials

Sodium borohydrate ≥98.5% was purchased from Sigma–Aldrich. Anhydrous ethanol 99.8% p.a. was obtained from Eurochem BGD. Chloric acid 35–38% p.a., nitric acid 65% p.a., acetone 99.5% p.a. were obtained from Chempur. Sulfuric acid 96% p.a. was purchased from Cheman. γ-Aminopropyltriethoxysilane 99% was purchased from Aldrich.

2.2. Preparation of MWCNTs

Multiwalled carbon nanotubes were synthesized by the chemical vapor deposition (CVD) method. The CVD synthesis method was described in details elsewhere

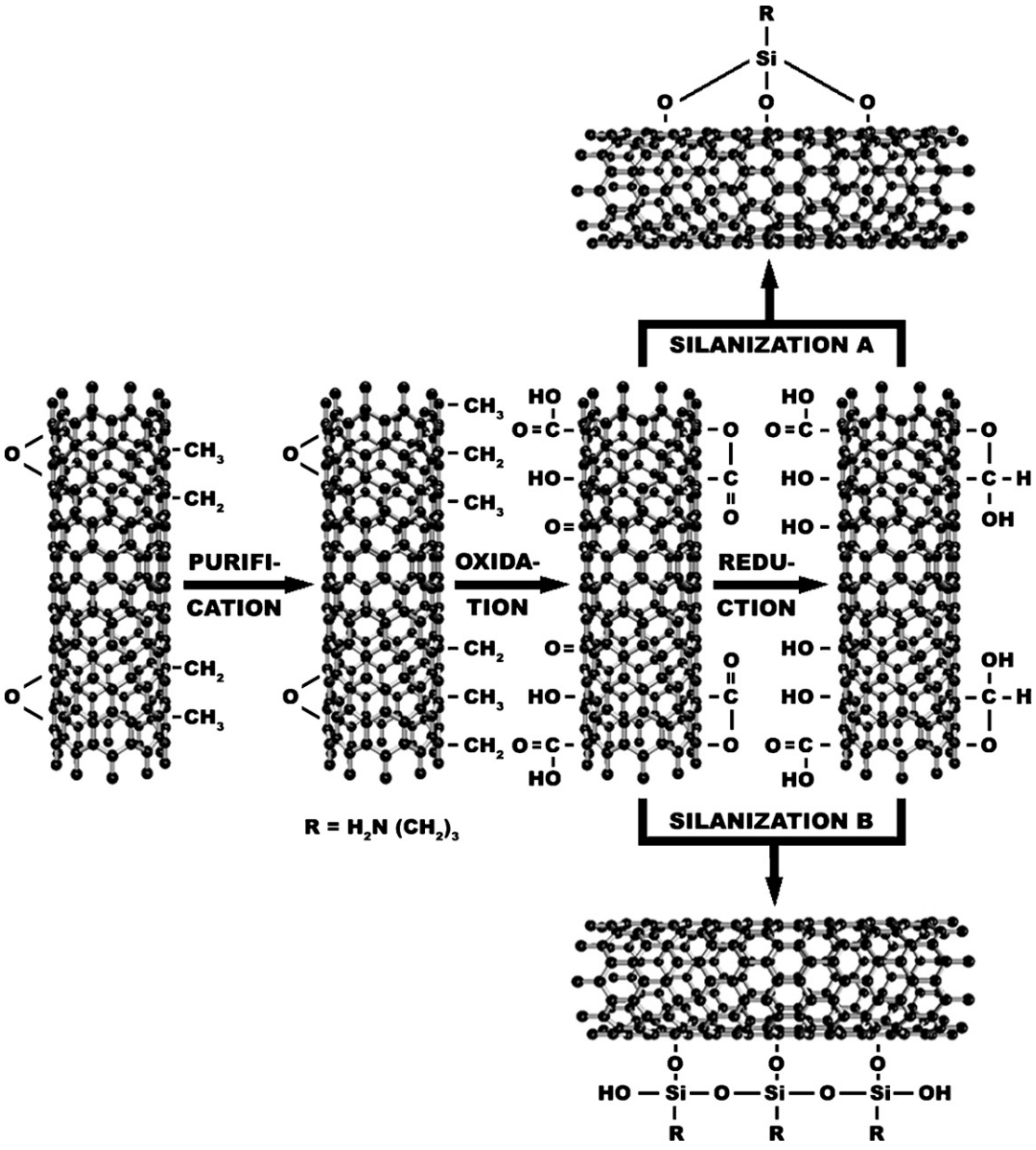

Fig. 1. Simplified representation of the experimental steps.

[34]. MWCNTs were purified by the chloric acid treatment in an ultra-sonication bath for 3 h. Next, the sample was subjected to the multiple filtration in order to remove impurities such as metal particles and the residual catalyst. Then MWCNTs were dried for 1 h. The purified sample (called pristine MWCNTs) (P-MWCNTs) was mixed with 80 ml mixture of 2.6 M HNO_3/2.6 M H_2SO_4 (v/v = 1:3). Then the sample was sonicated for 10 min and refluxed for 18 h at 175 °C. After this treatment, the mixture was neutralized with water after reversed osmosis process (RO H_2O) and filtrated through the polycarbonate filter (Whatman pore size 0.2 μm). Subsequently, the sample was rinsed thoroughly with RO H_2O and acetone. Then the oxidized MWCNTs (O-MWCNTs) were dried under vacuum at 180 °C for 1 h to degass adsorbed CO_2 and H_2O. A part of the oxidized MWCNTs was mixed with 200 ml of 99.8% anhydrous ethanol and sonicated in the ultra-sonication bath until dispersed. Then the sodium borohydrate powder (w/w = 5:1 $NaBH_4$/MWCNTs) was gently added into the solution and the mixture was placed onto a magnetic stirrer for 18 h at 4 °C. Subsequently, the mixture was filtrated through the polycarbonate filter and the sample was rinsed thoroughly with RO H_2O and acetone. Finally, the material was dried under vacuum for 1 h at 180 °C. This sample will be called reduced MWCNTs (R-MWCNTs).

2.3. Modification of functionalized MWCNTs surface

Two test tubes (Falcon - 50 ml) containing O-MWCNTs and two test tubes containing R-MWCNTs were prepared. The samples were mixed with RO H_2O and dispersed under vacuum in an ultra-sonication bath at 60 °C for 20 min. Next, the influence of two different silanization processes (A and B) on the O-MWCNTs and R-MWCNTs was tested. In Experiment A the solutions of the oxidized and reduced MWCNTs were filtrated through the polycarbonate filter and rinsed thoroughly with acetone. Then the obtained samples were redispersed in acetone solution in the test tubes connected to the vacuum pump and placed onto the magnetic stirrer. Next, APTES solution was gently added to the test tubes until its concentration of 2% was reached. Subsequently, the mixtures were stirred under vacuum for 15 min and were then left for 30 min in closed tubes at room temperature. The final solutions obtained in the silanization A reaction were well dispersed. They will be named OSA-MWCNTs and RSA-MWCNTs for the starting O-MWCNTs and R-MWCNTs, respectively. In Experiment B the solutions of the oxidized and reduced MWCNTs were filtrated through the polycarbonate filter and rinsed thoroughly with RO H_2O. Next, the obtained samples were redispersed in RO H_2O in the test tubes connected to the vacuum pump for 20 min at 40 °C in an ultra-sonication bath. Then the pH of the solutions was adjusted to 4.0 with known amount of glacial acetic acid. Afterwards, APTES solution was gently added to the test tubes until its concentration of 2% was reached. Subsequently, the mixtures were sonicated under vacuum for 15 min and then left for 3 h in closed tubes at 40 °C. The final products obtained in the silanization B reaction were poorly dispersed MWCNTs and will be named OSB-MWCNTs and RSB-MWCNTs for the starting O-MWCNTs and R-MWCNTs, correspondingly. In the next step all four mixtures were filtrated through a polycarbonate filter, rinsed with RO H_2O and acetone and dried on a hot plate at 50 °C.

2.4. Characterization of MWCNTs samples

Raman analysis was carried out using a micro-Raman Renishaw spectrometer (λ = 785 nm). For the investigation by the FT-IR spectroscopy [Nicolet 6700 FT-IR Spectrometer], the MWCNTs samples were dispersed in acetone in an ultra-sonication bath and prepared as a KBr pellets. The titration method proposed by Boehm was used to estimate the number of the surface functional groups. Thermogravimetric analysis was performed with 5 mg samples on DTA-Q600 SDT TA Instruments apparatus with the heating rate of 10 °C/min from room temperature to 900 °C in air. The morphological studies of the samples were conducted on a high-resolution transmission electron microscope (HRTEM) [FEI Tecnai F30] and their elemental compositions were detected with energy dispersive X-ray spectroscopy (EDX) as the microscope mode.

3. Results and discussion

After each experimental step, all the samples were investigated by the Raman spectroscopy. Raman spectra exhibit the D and G bands. The intensity of the D-band is proportional to the density of defects or surface functionalization [35]. Both effects allow the inelastic scattering needed for the single-phonon, double or triple resonance effects [36]. Therefore, Raman spectroscopy was used to determine the extent of functionalization which was estimated via calculation of the I_G/I_D ratio [37]. The I_G/I_D ratios from obtained Raman spectra of all investigated MWCNTs samples are shown in Fig. 2a.

The averaging I_G/I_D ratios were collected from several Raman spectra from different sample positions. The pristine MWCNTs (P-MWCNTs) exhibited the highest I_G/I_D ratio. From the results presented in Fig. 2a one can observe a gradual increase of the structural defects and/or surface moieties concentration after the oxidation (O-MWCNTs) and reduction (R-MWCNTs) processes. The acid treatment of MWCNTs led to the creation of new defect sites and destruction of the existing defects according to the mechanism of defect-consuming and defect-generation steps proposed by Zhang et al. [38]. These surface active sites containing hydroxyl functional groups, were anchoring points for the aminosilane molecules during the silanization process. The sodium borohydrate treatment of the oxidized sample led to the increase of hydroxyl group content by the reduction of the previously introduced lactone and carbonyl functional groups. From the results presented in Fig. 2a one can

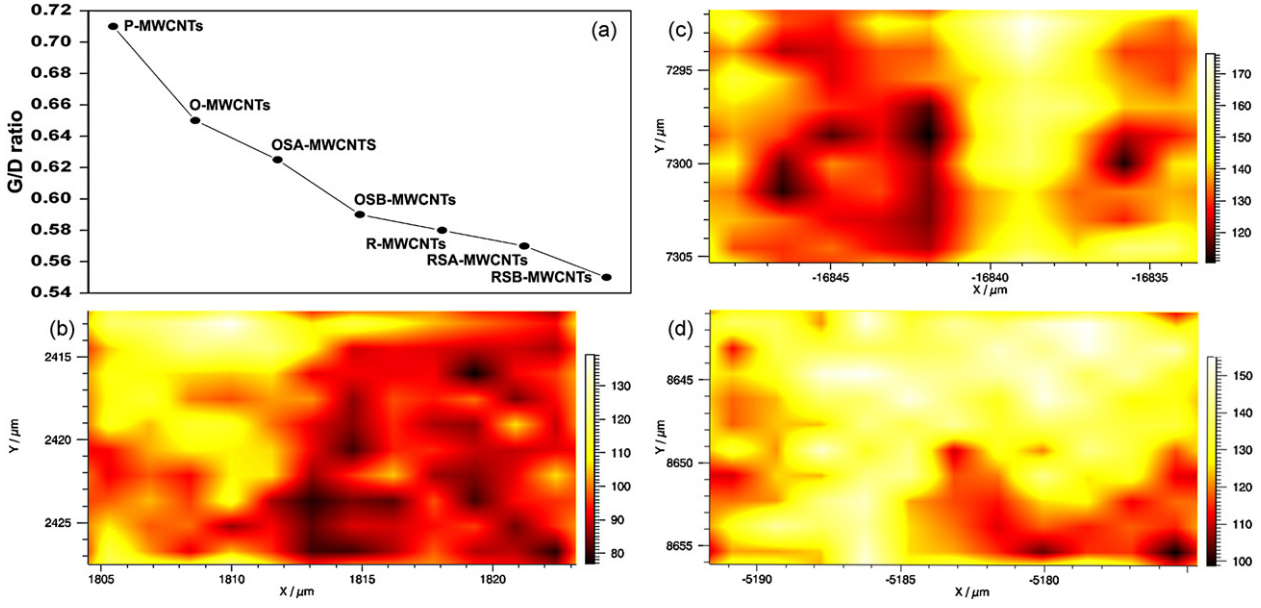

Fig. 2. I_G/I_D ratios from the Raman spectra of all investigated MWCNTs samples (a) and Raman 2D microscope images of the P-MWCNTs (b), OSB-MWCNTs (c), and RSB-MWCNTs (d).

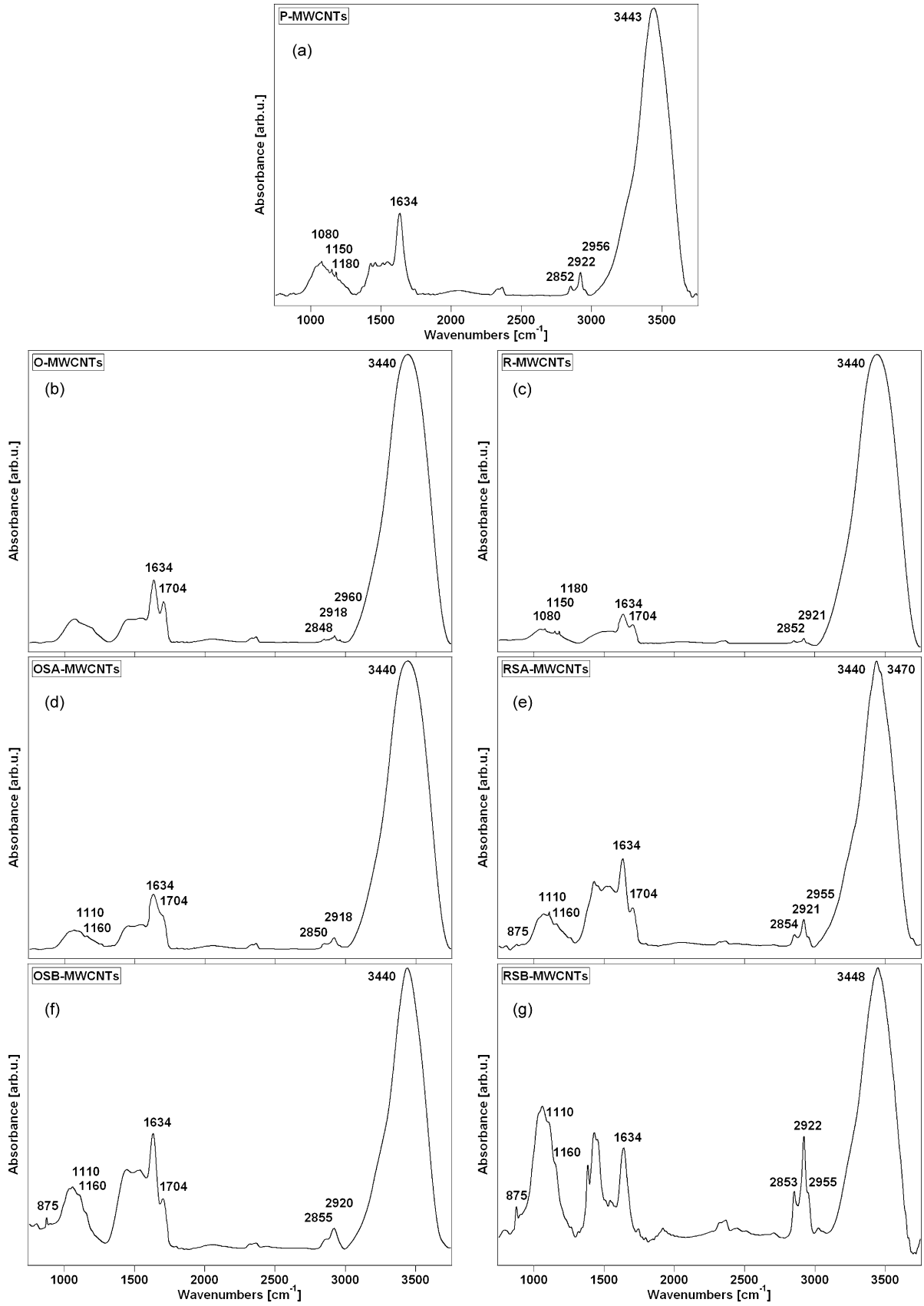

Fig. 3. FT-IR spectra of pristine (a), oxidized (b), reduced (c), OSA (d), RSA (e), OSB (f), and RSB (g) MWCNTs samples.

notice that the vibrational properties of the silanized MWCNTs had been significantly modified. The decrease of the I_G/I_D ratios in the case of OSA/RSA-MWCNTs and OSB/RSB-MWCNTs samples after the oxidation and reduction processes are closely related to the exohedral grafting of the silane molecules onto MWCNTs surface. The difference in the I_G/I_D ratio between OSA/RSA-MWCNTs and OSB/RSB-MWCNTs samples is due to the aminosilane condensation process which occurred in the silanization B process. This difference indicates that the hydrolysis process of APTES molecules provided a higher functionalization extent onto MWCNTs surface. Fig. 2b–d shows the Raman 2D maps of the distribution of D-mode in each sample: the pristine sample (b) OSB-MWCNTs (c), and RSB-MWCNTs (d). The darker area observed in the map corresponds to the lower intensity of D peak. For the pristine sample (Fig. 2b), the inhomogeneous distribution of the defect mode response is detected. The highly silanized samples (Fig. 2c and d) exhibit the increase of the D-mode intensity and increase of the homogeneity of D-mode distribution. Additionally, the distribution of this peak in RSB-MWCNTs sample (Fig. 2d) is much more homogeneous than in the OSB-MWCNTs sample (Fig. 2c) which could be due to the higher content of the attached molecules on the nanotubes surface.

Furthermore, FT-IR spectroscopy was used for the identification of the surface functional groups and exohedral functionalization by aminosilane molecules in all investigated samples (Fig. 3). In the presented spectra, the background was subtracted and normalized to the peak at 3440 cm^{-1}. The spectra of all the investigated sample exhibited C=C bonds at 1634 cm^{-1} and high narrow peak of O–H functional groups at ~3440 cm^{-1}. In most of the observed spectra, asymmetric methyl stretching band at ~2960 cm^{-1} and asymmetric/symmetric methylene stretching bands at ~2920 cm^{-1} and ~2850 cm^{-1} were observed, respectively. The intensities of these bands decreased in the optical response of the oxidized sample due to the formation of oxygen containing functional groups—mainly COOH whose vibrational response could be observed at 1704 cm^{-1} (Fig. 3b). In the spectra of the silanized samples (Fig. 3d–g), the intensity of CH_2 groups increased along with the amount of the bonded aminosilane molecules due to the presence of the surface aminopropyl moieties. Additionally, the vibrational response of the carboxylic groups decreased along with increase of the surface coating. The spectra of the pristine and reduced MWCNTs sample (Fig. 3a and c) exhibits C–O bond at 1180 cm^{-1} and asymmetric stretching bands at 1151 cm^{-1} and 1080 cm^{-1} which are associated with ether type groups. The disappearance of these bands at oxidized MWCNTs sample (Fig. 3b) could be caused by the cleavage of the C–O bond of the C–O–C fragment in the ether type functional groups by the nitric and sulfuric acid mixture. The reappearance of these groups at the spectrum of the reduced sample (Fig. 3c) could be a consequence of the $NaBH_4$ treatment process in which the reduction of the lactone groups into hydroxyl groups leads to the creation of the ether type groups. The grafting of the aminosilane molecules onto MWCNTs surface in all silanized samples was confirmed by the presence of the siloxyl (Si–O–C) bonds at 1110 cm^{-1} and Si–OH stretch mode at 875 cm^{-1}, respectively. The presence of the siloxane (Si–O–Si) bonds at 1161 cm^{-1} confirmed the occurrence of the condensation process. The intensity of these bands is related to the amount of the aminosilane molecules grafted on the surface. Additionally, at the spectrum of the RSA-MWCNTs (Fig. 3e) one can clearly see the band at 3470 cm^{-1} related to hydrogen-bonded silanols, however, in the remaining silanized samples, that the band could be screened due to the overlapping with peak related to –OH functional groups at ~3440 cm^{-1}.

The concentration of the functional groups content was estimated by modified Boehm titration method [20,39]. The quantitative composition of the investigated functional groups onto oxidized and reduced MWCNTs surface is summarized in Table 1.

Table 1
The functional groups content of the oxidized and reduced MWCNTs samples estimated by the Boehm titrations.

Functional groups content	Oxidized MWCNTs (%) ($\times 10^{-3}$)	Reduced MWCNTs (%) ($\times 10^{-3}$)
Carboxyl	0.50	0.50
Lactone	1.48	0.00
Phenolic hydroxyl	0.20	0.20
Hydroxyl	0.22	0.62

The oxidation via acid treatment provided a low content of the hydroxyl groups which determine the amount of bonded aminosilane molecules onto MWCNTs surface in both silanization experiments. The following reduction of the lactone and carbonyl functional groups via $NaBH_4$ treatment led to an almost threefold increase in hydroxyl group content. Therefore, with the increase of the number of anchoring points for silanization process the increase in efficiency of the silanization process was also expected.

Thermogravimetric analysis of all the prepared samples presents the thermal stability of each sample fractions: amorphous carbon, weakly bonded aminosilane molecules and multiwalled carbon nanotubes. The thermal stability was monitored by the weight-loss during the heating process. The TG, DTG and Voigt fitting of DTG curves of the pristine, oxidized and reduced samples obtained in thermogravimetric analysis are presented and described in details elsewhere [20]. Briefly, Table 2 summarizes the oxidation temperatures (T_o) and the calculations of the areas under the peaks corresponding to different fractions from DTG and Voigt fitting of DTG curves.

The Fraction I of the pristine sample (Table 2) corresponds to burning off the amorphous carbon. The ash content left after the thermoanalysis of P-MWCNTs sample was 4.6 wt%, O-MWCNTs and R-MWCNTs < 0.1 wt%, respectively. The disappearance of Fraction I in O-MWCNTs (Table 2) along with minimal ash content left, leads to the conclusion that amorphous carbon and remaining catalysts particles were removed via the oxidative acid treatment. The remaining fractions from P-MWCNTs, O-MWCNTs and R-MWCNTs samples correspond to the multiwalled carbon nanotubes with a different type and content of defects and/or functional groups.

In Fig. 4 presenting the thermogravimetric analysis of the silanized MWCNTs samples the bold, dash and dot lines correspond to the TG, DTG and Voigt fitting of DTG curve, respectively.

The DTG curve of the OSA-MWCNTs sample in Fig. 4a presents four stepwise weight-losses. An oxidation temperature of the Fraction I corresponds to the oxidation temperature of the weakly bonded aminosilane molecules to MWCNTs surface, while T_o of the Fractions II, III and IV correspond to T_o of the silanized MWCNTs. The calculations of the areas under the peaks corresponding to these fractions are indicated in the inset of this figure. One can notice the slight differences between T_o of the silanized MWCNTs from Fig. 4a and T_o of the fractions of O-MWCNTs sample from Table 2. The TG curve presented in Fig. 4a indicates the increase of the total mass left after the thermal analysis up to 3.13 wt%. This can be attributed to the silicon which is stable at high temperature and remained after the thermogravimetric analysis.

Table 2
The data obtained from DTG and Voigt fitting of DTG of the investigated samples.

Fractions in DTG	P-MWCNTs		O-MWCNTs		R-MWCNTs	
	Temp. (°C)	Area (%)	Temp. (°C)	Area (%)	Temp. (°C)	Area (%)
1	380	1.52	–	–	372	13.32
2	507	33.58	489	29.84	405	14.67
3	530	30.28	515	22.64	440	43.79
4	550	34.62	547	47.52	457	28.22

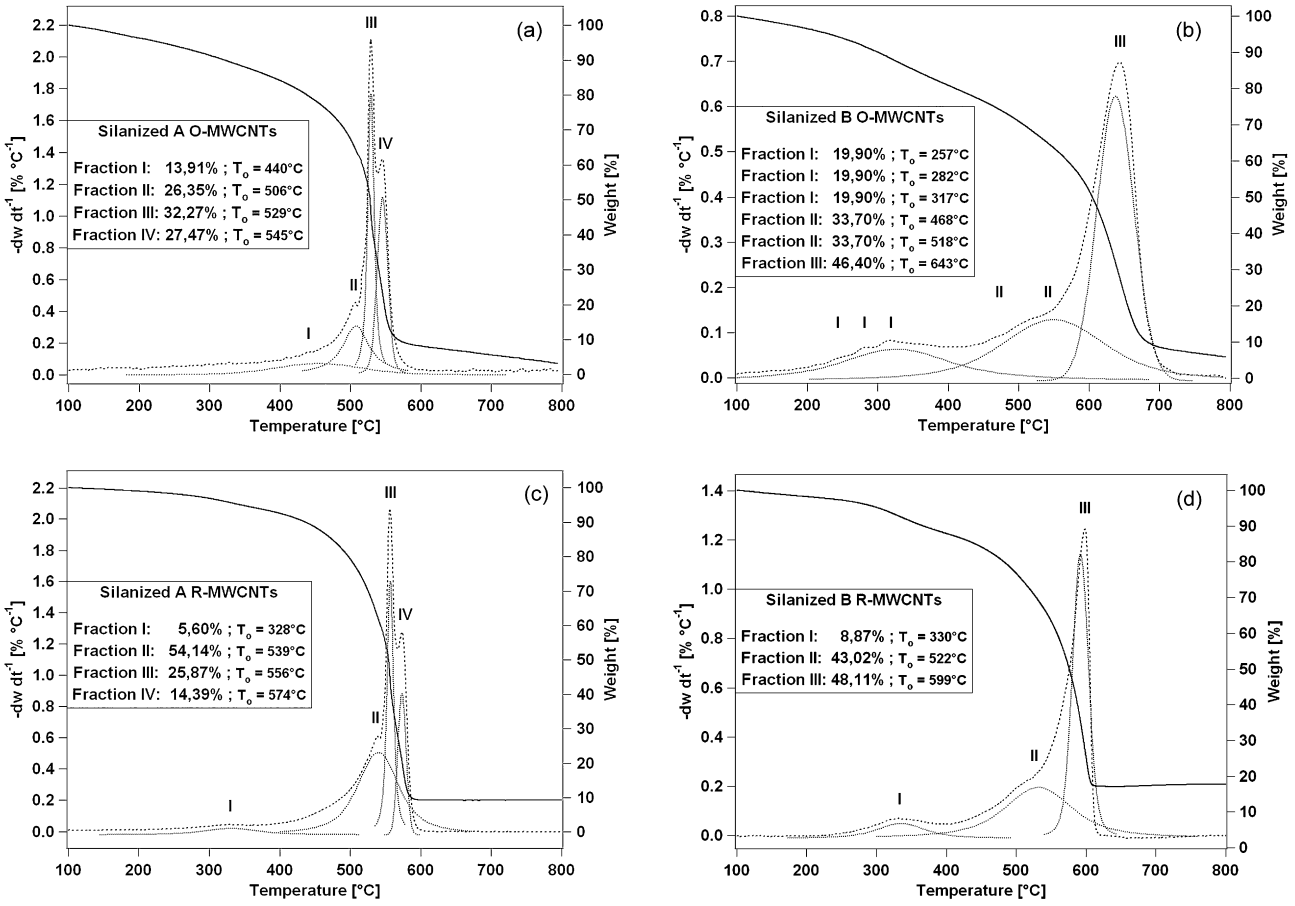

Fig. 4. TGA curves of the OSA (a), OSB (b), RSA (c), and RSB (d) MWCNTs samples.

The DTG curve of the OSB-MWCNTs sample in Fig. 4b exhibited three main stepwise weight-losses. Fraction I contains three consecutive weight-losses which correspond to the weakly bonded condensed aminosilane molecules. The presence of the two consecutive weight-losses in Fraction II seems to be an overlap of the burning off of O-MWCNTs and grafted aminosilane with the higher condensation degree, in comparison to the condensed aminosilane molecules burnt off in Fraction I. The strongest Fraction III corresponds to the O-MWCNTs with the abundance of well condensed aminosilane attached to the outer nanotube walls. The last fraction of the OSB-MWCNTs indicates highly improved thermal stability of the analyzed sample (T_o = 643 °C) which is 96 °C higher than T_o of the Fraction III of the oxidized multiwalled carbon nanotubes (Table 2). The TG curve in Fig. 4b indicates that the total mass left after the thermal analysis increased up to 5.89 wt%. This can be explained by the fact that the condensation process influenced the level of MWCNTs silanization.

In Fig. 4c four stepwise weight-losses of RSA-MWCNTs sample can be observed. Fraction I corresponds to the combustion of aminosilane molecules, while Fractions II, III and IV correspond to the combustion of the reduced MWCNTs with a high degree of the APTES grafting. The high level of the surface functionalization led to the significant T_o increase which is over 117 °C higher than T_o of the reduced MWCNTs fractions. The TG curve in Fig. 4c indicates that the total mass left after the thermal analysis is 9.30 wt% which is 6.17 wt% higher than the total mass which was left in OSA-MWCNTs sample. Both effects can be explained by the fact that higher amount of hydroxyl groups created during the reduction process provided more active sites for aminosilane molecules.

Finally, the DTG curve of the RSB-MWCNTs sample in Fig. 4d exhibited three stepwise weight-losses. Fraction I corresponds to the burning off of the weakly bonded condensed APTES molecules. Fraction I of the RSB-MWCNTs sample presents a very similar oxidation temperature to the Fraction I RSA-MWCNTs sample. However, in the RSB-MWCNTs sample the amount of the aminosilane is higher (3.27%) due to the condensation process. Fractions II and III correspond to the reduced MWCNTs featured by the strong grafting of the condensed aminopropyl-functional resinous polymer. The surface condensation of APTES in Fraction III of the RSB-MWCNTs sample led to the significant increase of the T_o which is 142 °C higher than T_o of Fraction IV of the R-MWCNTs sample (Table 2). The TG curve in Fig. 4d indicates the consecutive increase of the total mass left after the burning process (17.7 wt%).

Overall, based on data presented in Table 2 and Fig. 4 one can deduce that the fractions of the silanized MWCNTs whose T_o is in the range of 250–470 °C are attributed to the combustion of the APTES and decomposition of weakly bonded aminosilane molecules with different state of condensation. It is suggested that above 470 °C the thermal decomposition of the strong Si–O links to the nanotubes surface occurs. In comparison to the last fraction of the P-MWCNTs sample, the oxidation temperatures of the last

Table 3
The elemental composition of all investigated MWCNTs samples by EDX analysis.

Sample	C (wt%)	O (wt%)	Si (wt%)	N (wt%)
Pristine MWCNTs	97.91	2.09	0.0	0.0
Oxidized MWCNTs	62.84	37.16	0.0	0.0
Reduced MWCNTs	59.76	40.24	0.0	0.0
Silanized A O-MWCNTs (OSA)	94.85	2.02	2.28	0.85
Silanized B O-MWCNTs (OSB)	90.95	2.87	3.44	2.74
Silanized A R-MWCNTs (RSA)	87.50	4.24	4.56	3.70
Silanized B R-MWCNTs (RSB)	82.18	9.04	4.95	3.83

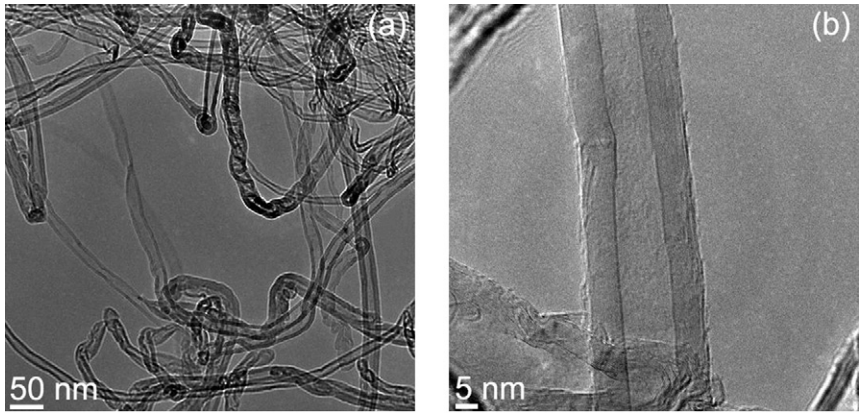

Fig. 5. TEM micrographs of pristine MWCNTs bundles (a) and individual nanotube (b).

fractions of the OSB-MWCNTs and RSB-MWCNTs samples exhibited improved thermostability up to 93 °C and 49 °C, respectively.

The energy dispersive X-ray (EDX) analysis was used to characterize the elemental composition of all investigated MWCNTs samples. Table 3 presents the weight percentage of the carbon, oxygen, silicon and nitrogen in pristine, oxidized, reduced and silanized MWCNTs samples. The increased amount of silicon atoms (almost 5%) obtained in analysis of the RSB-MWCNTs sample could be a significant evidence of the surface covalent modification which is clearly related to the high amount of the hydroxyl groups in the reduced MWCNTs sample and condensation of the aminosilane molecules during silanization process.

Fig. 5 reveals the morphology of the pristine MWCNTs in a larger fraction of the sample (a) and the closeup of the individual tube (b). One can clearly see that the presented structure exhibits typical multiwalled carbon nanotubes characteristics. Detailed microscopic analysis proved that almost no amorphous carbon was detected in all the observed sample areas. This observation was confirmed in high-resolution TEM observation. The individual tube shows a well-organized cylindric graphene layers without only a few amorphous species in or out of the tube.

The TEM analysis of the functionalized samples is depicted in Fig. 6: the oxidized sample (a), OSA (b), OSB (c), the reduced sample (d), RSA (e) and RSB (f). The microscopic analysis allows one to observe the morphological changes in each sample. The samples were compared to the pristine sample. After each step of the functionalization the presence of some additional structures, mostly on the nanotubes surface, were detected. This can be attributed to the introduction of the respective functional groups and aminosilane molecules. This effect is the most pronounced in the sample after the oxidation followed by the reduction process and silanization in hydrolysis conditions (RSB-MWCNTs) seen in Fig. 6f. Here, one can see even the whole tubes being coated presumably by the condensed aminopropyl moieties.

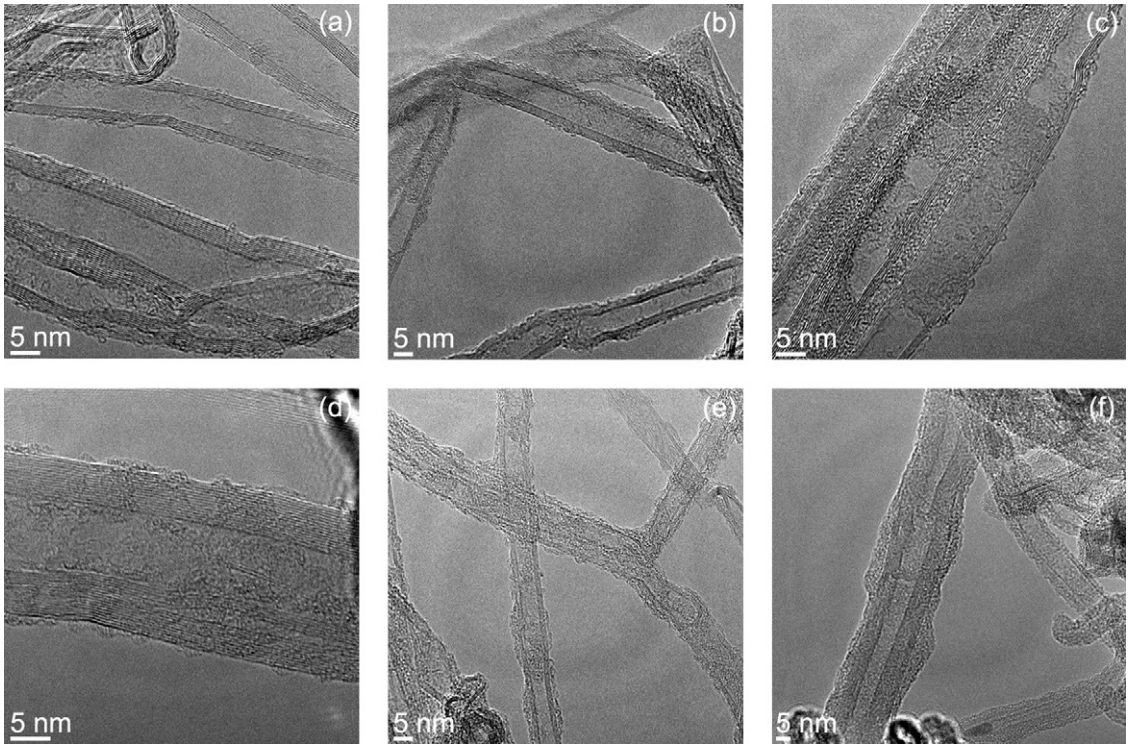

Fig. 6. TEM micrographs of oxidized (a), OSA (b), OSB (c), reduced (d), RSA (e), RSB (f) MWCNTs samples.

4. Conclusions

The influence of the different silanization routes on the thermal, structural and vibrational properties of MWCNTs has been presented. The detailed spectroscopic, thermogravimetric, and microscopic analyses of the samples at each step of the preparation have been shown. As it was observed, the thermal stability of MWCNTs decreased along with the increase of the functionalization by surface moieties. Interestingly, it was proved that the silanization process enhances the thermal stability of MWCNTs. This effect is clearly visible in the oxidized and reduced samples silanized via the condensation process of the aminosilane molecules on the MWCNTs surface. Moreover, the silanization B route of the oxidized followed by the reduction MWCNTs forms homogenous layer of aminopropyl-functional polymer around its outer walls. This efficient functionalization leads to the obtaining of MWCNTs matrix which due to the abundance of free NH_2 functional groups could be used as a matrix for the immobilization of enzymes, drugs and as a part of polymer nanocomposites.

Acknowledgments

The authors wish to acknowledge the assistance provided by A. Bachmatiuk, A. Jędrzejewska and S. Costa. The work was funded by Polish research grant in 2009–2012.

References

[1] F. Xue, S. Jiehe, F. Yan, C. Wei, Mater. Sci. Eng. A 527 (2010) 1586–1589.
[2] N.G. Sahoo, H.K.F. Cheng, L. Li, S.H. Chan, Z. Judeh, J. Zhao, Adv. Funct. Mater. 19 (2009) 3962–3971.
[3] Q. Li, C. Liu, S. Fan, Nano Lett. 9 (2009) 3805–3809.
[4] H. Qian, A. Bismarck, E.S. Greenhalgh, M.S.P. Shaffer, Comp. Sci. Technol. 70 (2010) 393–399.
[5] R. Ormsby, T. McNally, C. Mitchell, N. Dunne, J. Mech. Behav. Biomed. Mater. 3 (2010) 136–145.
[6] F. Yu, H. Cai, W. He, W. Yang, Z. Xie, J. Appl. Polym. Sci. 115 (2009) 2946–2954.
[7] T.P. Chua, M. Mariatti, A. Azizan, A.A. Rashid, Comp. Sci. Technol. 70 (2010) 671–677.
[8] J. Ryu, H.S. Kim, H.T. Hahn, D. Lashmore, Biosens. Bioelectron. 25 (2010) 1603–1608.
[9] Y. Zhang, X. Sun, L. Pan, H. Li, Z. Sun, C. Sun, B.K. Tay, J. Alloys Compd. 480 (2009) L17–L19.
[10] W. Guo, L. Xu, F. Li, B. Xu, Y. Yang, S. Liu, Z. Sun, Electrochim. Acta 55 (2010) 1523–1527.
[11] X.G. Wang, Y.J. Fan, J. Appl. Electrochem. 39 (2009) 1451–1455.
[12] W.D. Zhang, J. Chen, L.C. Jiang, Y.X. Yu, J.Q. Zhang, Electrochim. Acta 168 (2010) 259–265.
[13] L. Kong, J. Wang, X. Fu, Y. Zhong, F. Meng, T. Luo, J. Liu, Carbon 48 (2010) 1262–1270.
[14] H. Kaman, A. Kukovecz, F. Simon, M. Holzweber, C. Kramberger, T. Pichler, Synth. Met. 141 (2004) 113–122.
[15] K. Kan, T. Xia, Y. Yang, H. Bi, H. Fu, K. Shi, J. Appl. Electrochem. 40 (2010) 593–599.
[16] I. Baravik, R. Tel-Vered, O. Ovits, I. Willner, Langmuir 25 (2009) 13978–13983.
[17] M.V. Naseh, A.A. Khodadadi, Y. Mortazavi, F. Pourfayaz, O. Alizadeh, M. Maghrebi, Carbon 48 (2010) 1369–1379.
[18] H. Liu, X. Wang, P. Fang, S. Wang, X. I, C. Pan, G. Xie, K.M. Liew, Carbon 48 (2010) 721–729.
[19] B. Vigolo, C. Hérold, J.F. Marêché, J. Ghanbaja, M. Gulas, F. Le Normand, R. Almairac, L. Alvarez, J.L. Bantignies, Carbon 48 (2010) 949–963.
[20] B. Scheibe, E. Borowiak-Palen, R.J. Kalenczuk, Mater. Character. 61 (2010) 185–191.
[21] Y.C. Chiang, C.C. Lee, C.Y. Lee, Toxicol. Environ. Chem. 91 (2009) 1413–1427.
[22] Z. Wang, M.D. Shirley, S.T. Meikle, R.L.D. Whitby, S.V. Mikhalovsky, Carbon 47 (2009) 73–79.
[23] P. Liu, T. Wang, Appl. Phys. A 97 (2009) 771–775.
[24] H.C. Kim, S.K. Kim, J.T. Kim, K.Y. Rhee, J. Kathi, J. Macromol. Sci. B 49 (2010) 132–142.
[25] L. Liu, Y. Qin, Z.X. Guo, D. Zhu, Carbon 41 (2003) 331–335.
[26] J.K. Kim, D.Z. Wo, L.M. Zhou, H.T. Huang, K.T. Lau, M. Wang, Key Eng. Mater. 334–335 (2007) 797–800.
[27] Z. Zhou, S. Wang, L. Lu, Y. Zhang, Y. Zhang, Compos. Sci. Technol. 68 (2008) 1727–1733.
[28] P.C. Ma, J.K. Kim, B.Z. Tang, Compos. Sci. Technol. 67 (2007) 2965–2972.
[29] J. Kathi, K.Y. Rhee, J. Mater. Sci. 43 (2008) 33–37.
[30] J.T. Kim, H.C. Kim, S.K. Kim, J. Kathi, K.Y. Rhee, J. Comp. Mater. 43 (2009) 2533.
[31] J.H.T. Luong, S. Hrapovic, D. Wang, F. Benseba, B. Simard, Electroanalysis 16 (2004) 132–139.
[32] J.H.T. Luong, S. Hrapovic, D. Wang, Electroanalysis 17 (2005) 47–53.
[33] M. Yamaura, R.L. Camilo, L.C. Sampaio, M.A. Macedo, M. Nakamura, H.E. Toma, J. Magn. Magn. Mater. 279 (2004) 210–217.
[34] E. Borowiak-Palen, A. Bachmatiuk, M.H. Rümmeli, T. Gemming, M. Kruszynska, R.J. Kalenczuk, Phys. E: Low-Dim. Syst. Nanostr. 40 (2008) 2227–2230.
[35] W.J. Kim, M.L. Usrey, M.S. Strano, Chem. Mater. 19 (2007) 1571–1576.
[36] A.C. Dillon, P.A. Parilla, J.L. Alleman, T. Gennett, K.M. Jones, M.J. Heben, Chem. Phys. Lett. 401 (2005) 522–528.
[37] S. Costa, E. Borowiak-Palen, M. Kruszynska, A. Bachmatiuk, R.J. Kalenczuk, Mater. Sci. Pol. 26 (2008) 2.
[38] J. Zhang, H. Zou, Q. Qing, Y. Yang, Q. Li, Z. Liu, X. Guo, Z. Du, J. Phys. Chem. B 107 (2003) 3712–3718.
[39] H.P. Boehm, Advances in Catalysis, Academic Press, 1966, pp. 179–274.